

Restricted phase-space approximation in real-time stochastic quantization

Ryoji Anzaki^a Kenji Fukushima^b Yoshimasa Hidaka^c and
Takashi Oka^a

^a*Department of Applied Physics, The University of Tokyo, 7-3-1 Hongo,
Bunkyo-ku, Tokyo 113-0033, Japan*

^b*Department of Physics, The University of Tokyo, 7-3-1 Hongo, Bunkyo-ku, Tokyo
113-0033, Japan*

^c*Theoretical Research Division, Nishina Center, RIKEN, Wako 351-0198, Japan*

Abstract

We perform and extend real-time numerical simulation of a low-dimensional scalar field theory or a quantum mechanical system using stochastic quantization. After a brief review of the quantization method and the complex Langevin dynamics, we calculate the propagator and make a comparison with analytical results. This is a first step toward general applications, and we focus only on the vacuum properties of the theory; this enables us to handle the boundary condition with the $i\epsilon$ prescription in frequency space. While we can control stability of the numerical simulation for any coupling strength, our results turn out to flow into an unphysical fixed-point, which is qualitatively understood from the corresponding Fokker-Planck equation. We propose a simple truncation scheme, “restricted phase-space approximation,” to avoid the unphysical fixed-point. With this method, we obtain stable results at reasonably good accuracy. Finally we give a short discussion on the closed-time path formalism and demonstrate the direct computation of the vacuum expectation value not with the $i\epsilon$ prescription but from an explicit construction of the Feynman kernel.

Key words: Real-time dynamics, Numerical simulation, Scalar field theory, Stochastic quantization, Complex Langevin equation

1 Introduction

Large-scale numerical computation is becoming a vital building block in today’s scientific researches. In theoretical physics, the numerical approach is

regarded as a starting point of a pursuit toward fundamental understanding of new phenomena. Performing numerical *experiments*, we can test ideas and hypotheses in an ideal setup repeatedly and easily, which is usually difficult in real experiments. This enables us to efficiently build models and theories that describe nature. In this spirit, in order to study new physics, it is important to develop new numerical methods and extend their validity.

Quantum field theories that accommodate infinite degrees of freedom stand in the center of modern physics. It is becoming less and less costly to perform large-scale numerical simulations thanks to tremendous developments in the computing power and the various innovations in the numerical algorithms. One area where computers are playing an important role is the fundamental theory of the strong interaction; that is, quantum chromodynamics (QCD) [1] can be formulated on the four-dimensional lattice grid in Euclidean space-time, so that the exponentiated action, $e^{-S_{\text{QCD}}}$, is a real positive number and can be interpreted as a weight factor in analogy with statistical mechanics [2]. We can then carry out the functional integral by means of the Monte-Carlo algorithm as long as the weight factor is real and non-negative. This approach known as the lattice-QCD simulation [3] has been the most successful non-perturbative tool to investigate the QCD-vacuum (topological) structure [4], thermodynamics of QCD matter [5,6], the hadron spectroscopy [7], and also the real-time characters such as the spectral function [8,9], the particle production rate [10,11], and the transport coefficients [12,13,14,15,16], etc.

Another area where numerical simulations are intensively utilized is condensed matter physics, especially in the field of strongly correlated electron systems. It has been realized that quantum many-body effect leads to various phase transitions. A well studied example is the Mott transition [17] in which electrons freeze their motion due to strong Coulomb interaction. It is believed that this transition is relevant to understanding of the pairing mechanism of high temperature superconductivity [18]. Numerical algorithms such as the density matrix renormalization group (DMRG) [19,20] and the dynamical mean field theory (DMFT) [21] have been developed and applied to problems in correlated electron systems. Recently, real-time dynamics in condensed matter systems is becoming a hot topic (for a review see Ref. [22]). One important problem is the physics of quantum quench; i.e., many-body dynamics triggered by a rapid parameter change. Phenomena such as “prethermalization” [23], initially discovered in the QCD community, has motivated many condensed matter researches [24,25]. In condensed matter, variety of methods exist to deal with the problem of a time-evolving quantum many-body system. They range from direct wave-function-based techniques such as exact diagonalization and DMRG [26,27,28], quantum master equations [29], and quantum kinetic equations [30], to the Keldysh formalism for the non-equilibrium Greens functions [31,32,33]. Using the Keldysh formalism, many sophisticated theoretical techniques that were developed for equilibrium can be straightforwardly

Method	Quantum	Variables	Limitation
Stochastic quantization	Full	Fields $\phi(x, t, \theta)$	Unphysical fixed-point
Classical statistical sim.	$\mathcal{O}(\hbar)$	Fields $\phi(x, t)$	Large occupation num.
Real-time QMC	Full	Green's func.	Sign problem
Time-dependent DMRG	Full	Wave function	Low-dim systems
Non-equilibrium DMFT	Full	Green's func.	Short time

Table 1

Numerical methods for real-time calculations. The classical statistical simulation contains quantum fluctuations only up to $\mathcal{O}(\hbar)$ but the long-time simulation is possible, while other methods are fully quantum. Each method has an advantage and a limitation of the validity as listed.

utilized to non-equilibrium systems; e.g., diagrammatic quantum Monte-Carlo method (QMC) [34,35] and non-equilibrium DMFT [22,36]. The price to pay is the severe negative sign problem, and it is still challenging to study the long time behavior. We summarize major approaches for non-equilibrium many-body systems in Table 1.

In order to study non-linear QCD processes far from equilibrium such as the pattern formation [37] and the turbulent flow [38], a method that can treat not only fermions but also bosons must be developed. To overcome the limitation of the Monte-Carlo simulation, some alternative approaches are proposed such as the gauge/gravity correspondence [39], the classical statistical field theory [40,41,42], the 2-particle-irreducible formalism [43] (see also Ref. [31]), and the stochastic quantization [44,45,46,47].

The gauge/gravity correspondence has provided us with useful insights into the thermalization problem and the numerical simulations are possible now to trace the evolution processes of the dynamical system [48,49,50,51,52,53,54], though the technique can be applied only to a special class of the strong-coupling gauge theory. The classical statistical simulation, which is also known as the ‘‘truncated Wigner’’ approximation [55], is quite successful in describing the early stages of the relativistic heavy-ion collision [56,57,58,59], which has been closely investigated in connection to the wave turbulence and the scaling behavior also [60,61,62,63,64,65,66,67,68].

Although the classical statistical simulation is a useful tool in the regime where the occupation number is large enough to justify the classical treatment, the formalism itself needs to be elaborated not to ruin the renormalizability [69]. For this purpose it is an interesting question to think of a possible relation between the classical statistical approach and stochastic quantization as speculated in Ref. [70], that has been hinted also by the simulation in Ref. [71].

Needless to say, if one can perform a direct real-time simulation with stochastic quantization without making any approximation, we can go beyond the limitation $\mathcal{O}(\hbar)$ of the classical statistical approximation. It should be intriguing to pursue such an ultimate goal.

There have been several attempts to solve the real-time theories using stochastic quantization numerically [72,73,74], which, however, did not succeed in proceeding far out of equilibrium. As we will explain later, we should then solve a diffusion equation with a pure-imaginary coefficient together with stochastic random variables; i.e., a complex Langevin equation [75,76]. We are often stuck with two major obstacles in handling the complex Langevin equation: one is the numerical instability, and the other is the problem of run-away trajectories (i.e., physical instability). Not only in the context of real-time physics, but also in the efforts to attack the so-called sign problem at finite density [77], the adaptive step-size method is developed to suppress the numerical instability and the convergence is under careful investigation [78,79]. The stochastic quantization method has also been utilized in the application of the Lefschetz thimble to evade the sign problem [80,81,82,83,84].

Because the theoretical interest in the potential of stochastic quantization is growing lately in various research fields, it is quite timely to revisit this method to perform a direct real-time simulation. In this paper we do not assume that the initial state is in thermal equilibrium (which will enhance stability of the simulation [73]) but limit ourselves to the vacuum properties only, for which the information on the initial and final wave-functionals are to be dropped by the $i\epsilon$ prescription. Besides, we can check if our numerical results are on the right physical trajectory or not as long as the vacuum properties are somehow known. Our ultimate goal shall be the study of full quantum and non-equilibrium phenomena, and in the final section, we will briefly sketch an outlook along these lines.

2 Scalar Field Theory in Minkowski Space-time

To make our discussions self-contained, we shall make a brief overview of stochastic quantization here for a real scalar field theory (see reviews [46,47] for more details). Readers who are familiar with real-time formalism and stochastic quantization can skip this section and jump to Sec. 3.

2.1 Formalism

Let us begin with the general formulation of quantum field theory. We denote the amplitude from the initial $|\Psi_i, t_i\rangle$ to the final $|\Psi_f, t_f\rangle$ as $\langle\Psi_f, t_f|\Psi_i, t_i\rangle$, which we can rewrite in the functional integral form as follows:

$$\langle\Psi_f, t_f|\Psi_i, t_i\rangle = \langle\Psi_f|e^{-iH(t_f-t_i)}|\Psi_i\rangle = \int\mathcal{D}\phi e^{iS[\phi]}\Psi_f^*[\phi(t_f)]\Psi_i[\phi(t_i)] \quad (1)$$

with H being the Hamiltonian. Then, the n -point Green's functions read:

$$\begin{aligned} G^{(n)}(x_1, x_2, \dots, x_n; t_f; \Psi_f, t_f; \Psi_i, t_i) \\ &\equiv \frac{1}{\langle\Psi_f, t_f|\Psi_i, t_i\rangle} \langle\Psi_f, t_f|T\phi(x_1)\phi(x_2)\cdots\phi(x_n)|\Psi_i, t_i\rangle \\ &= \frac{\int\mathcal{D}\phi e^{iS[\phi]}\Psi_f^*[\phi(t_f)]\Psi_i[\phi(t_i)]\phi(x_1)\phi(x_2)\cdots\phi(x_n)}{\int\mathcal{D}\phi e^{iS[\phi]}\Psi_f^*[\phi(t_f)]\Psi_i[\phi(t_i)]}, \end{aligned} \quad (2)$$

where T denotes the time-ordered-product operator. These general Green's functions obviously depend on the choice of the initial and final wave functionals. Thus, for the calculation of the amplitude, the real-time evolution of quantum systems is formulated as the boundary problem rather than the initial-value problem as in classical physics. We are sometimes interested in the vacuum properties also, which can be accessed either by convoluting the vacuum wave-functional $\Psi_0[\phi]$ (see Eq. (35) for an explicit form and Fig. 1 (a) for an illustration) or by taking $t_f - t_i \rightarrow \infty$ with Feynman's $i\epsilon$ prescription (see Fig. 1 (b)): $H \rightarrow H(1 - i\epsilon)$. Inserting the complete set onto $e^{-iH(t_f-t_i)(1-i\epsilon)}|\Psi_i\rangle$, we can extract the dominant contribution in this limit as

$$\begin{aligned} e^{-iH(t_f-t_i)(1-i\epsilon)}|\Psi_i\rangle &= \sum_n e^{-iE_n(t_f-t_i)(1-i\epsilon)}|n\rangle\langle n|\Psi_i\rangle \\ &= e^{-iE_0(t_f-t_i)(1-i\epsilon)}|\Omega\rangle\langle\Omega|\Psi_i\rangle \left[1 + \mathcal{O}(e^{-(E_1-E_0)(t_f-t_i)\epsilon})\right]. \end{aligned} \quad (3)$$

Thus, the vacuum state $|\Omega\rangle$ dominates in the presence of small but finite ϵ . In this case, the Green's functions given in Eq. (2) become insensitive to any excited states but the vacuum state; i.e.,

$$G^{(n)}(x_1, x_2, \dots) = \langle\Omega|T\phi(x_1)\phi(x_2)\cdots\phi(x_n)|\Omega\rangle, \quad (4)$$

where the normalization of the vacuum is assumed to be $\langle\Omega|\Omega\rangle = 1$. In the numerical simulation, practically, $t_f - t_i$ cannot be infinity, and thus we need to keep $(E_1 - E_0)(t_f - t_i)\epsilon \gg 1$ to make the vacuum state dominate over any excited states. We present a schematic illustration in Fig. 1 to sketch these two alternative methods to extract the vacuum amplitude.

For more general problems out of equilibrium we often need an expectation

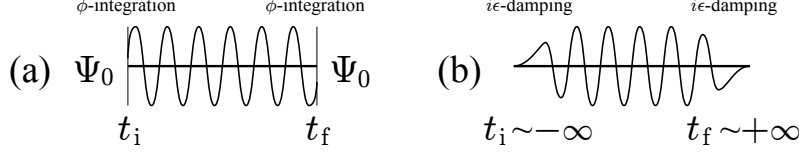


Fig. 1. Schematic illustration of the vacuum amplitude in two different but equivalent ways: (a) The convolution with the vacuum wave-functional Ψ_0 is taken at t_i and t_f . (b) The boundary is irrelevant for sufficiently large t_i and t_f as a result of the damping by $i\epsilon$.

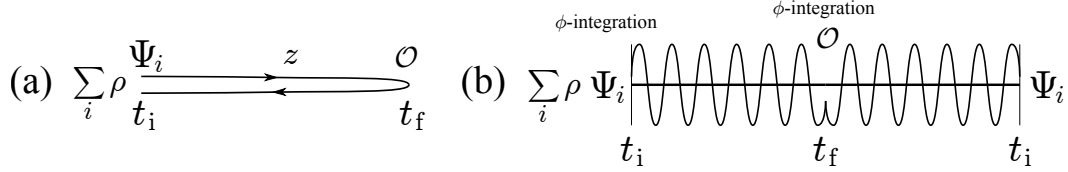


Fig. 2. Schematic illustration of the expectation value. (a) Representation in the closed-time path formalism by introducing a complexified time variable z . (b) Unfolded representation analogous to the amplitude calculations as depicted in Fig. 1.

value of some operator \mathcal{O} at t_f with an initial condition given at t_i , which we can express as

$$\langle \mathcal{O} \rangle_{t_f} \equiv \sum_{\Psi_i} \langle \Psi_i; t_i | \rho e^{-iH(t_i-t_f)} \mathcal{O} e^{-iH(t_f-t_i)} | \Psi_i; t_i \rangle. \quad (5)$$

Here the density matrix ρ specifies the initial state at t_i . Using a complexified time variable z , we can regard Eq. (5) as an “amplitude” computed on the closed-time path; see Fig. 2 (a). If the system is thermal and ρ takes a form of $\rho = e^{-H/T}/(\text{tr} e^{-H/T})$, it would be an elegant representation of the theory if we combine all time-evolution operators, $e^{-iH(t_f-t_i)}$, $e^{-iH(t_i-t_f)}$, and $e^{-H/T}$ together with z running along a single path on the complex plane. This is nothing but the real-time formalism of the finite-temperature field theory [85]. In this manner we can recover the well-known 2×2 matrix structure of the propagator from a combination of the forward ($t_i \rightarrow t_f$) and the backward path ($t_f \rightarrow t_i$). The off-diagonal components pick up ρ , and in the case of thermal equilibrium, they contain the thermal distribution function.

For a general ρ , we can no longer incorporate ρ as a deformation of the time path, and we should close the time path with an explicit insertion of the density matrix at initial t_i as sketched in Fig. 2 (a). This is the basic description of the closed-time path (CTP) or the Schwinger-Keldysh formalism [32,33]. We note that the closed-time path is often extended to $t_f = \infty$ for convenience especially when the perturbative calculation is formulated. Putting a source $J(z)$ along the path of Fig. 2 (a), we can construct an arbitrary operator by taking $\delta/\delta J(z)$.

As we will discuss in great details in Sec. 5, in stochastic quantization, we do not have to introduce the 2×2 matrix propagator. We can actually unfold the closed-time path as in Fig. 2 (b), so that we can perform direct numerical simulations to evaluate the expectation value in the same way as the amplitude calculation. One may think that the time evolution for $t_f \rightarrow t_i$ is just a duplicate of that for $t_i \rightarrow t_f$, and this is true as we see in Sec. 5, but this seemingly redundant reflection plays an important role for the treatment of a singular edge at t_f .

Let us now proceed to the formulation of stochastic quantization. In Euclidean field theories the weight appears in the functional integral (1) as a Boltzmann factor e^{-S_E} with the Euclidean action S_E . The stochastic process or the corresponding Fokker-Planck equation can generate such a weight correctly; in other words, quantum fluctuations are encoded in a form of the Langevin dynamics, which was proposed by Parisi and Wu [45] and is commonly called “stochastic quantization.” In Minkowski space-time, however, the weight factor e^{iS} takes a complex value and the convergence with the Fokker-Planck equation is a subtle problem, while the Langevin dynamics reproduces the ordinary perturbative series.

The real scalar field theory of our present interest is defined with the following action:

$$S = \int d^d x \left[\frac{1}{2} (\partial_\mu \phi)(\partial^\mu \phi) - \frac{m^2}{2} \phi^2 - \frac{\lambda}{4} \phi^4 \right], \quad (6)$$

where d is the number of space-time dimensions and we consider the ϕ^4 -interaction only. The corresponding (complex) Langevin equation turns out to be

$$\begin{aligned} \partial_\theta \phi(x, \theta) &= i \frac{\delta S}{\delta \phi(x)} \Big|_{\phi(x) \rightarrow \phi(x, \theta)} + \eta(x, \theta) \\ &= -i(\square + m^2 - i\epsilon) \phi(x, \theta) - i\lambda \phi^3(x, \theta) + \eta(x, \theta), \end{aligned} \quad (7)$$

where θ is the fictitious time not related to physical coordinates and it runs from 0 to ∞ in a conventional choice. We denote the stochastic noise term by $\eta(x, \theta)$.

We should fix a starting condition at $\theta = 0$ and the simplest prescription is $\phi(x, \theta = 0) = 0$. It is possible to choose a non-zero initial condition, but it will be vanishing at $\theta \rightarrow \infty$ and so irrelevant to the final results as long as we utilize the $i\epsilon$ prescription. To recover the ordinary perturbative expansion of the ϕ^4 -theory, the stochastic noise should satisfy

$$\langle \eta(x, \theta) \eta(x', \theta') \rangle_\eta = 2 \delta^{(d)}(x - x') \delta(\theta - \theta'). \quad (8)$$

In other words, the above expression gives us a definition of the average procedure over $\eta(x, \theta)$ as a Gaussian average. If we want to know the vacuum

expectation value of some operator \mathcal{O} , we should calculate the η -average of $\mathcal{O}[\phi(x, \theta)]$ where the η -dependence comes in through the θ -evolution of $\phi(x, \theta)$ according to Eq. (7). This means that

$$\langle \mathcal{O}[\phi(x)] \rangle = \lim_{\theta \rightarrow \infty} \langle \mathcal{O}[\phi(x, \theta)] \rangle_{\eta} . \quad (9)$$

Here, precisely speaking, the vacuum expectation value in the left-hand side represents the time-ordered quantity as usual in the functional integration formalism.

Now that we finish a quick flash of stochastic quantization, let us make sure that it certainly produces the ordinary perturbation theory, which also turns out to be useful for later discussions about the numerical simulation.

2.2 Recovery of the free propagator

It is the most convenient to move to the Fourier space to solve the complex Langevin equation (7) analytically. We define the scalar field and stochastic variables in momentum space as

$$\phi_k(\theta) \equiv \int d^d x \phi(x, \theta) e^{ik \cdot x} , \quad \eta_k(\theta) \equiv \int d^d x \eta(x, \theta) e^{ik \cdot x} \quad (10)$$

with the four-vector notation: $k \equiv (\omega, \mathbf{k})$. We can then recast the differential equation with $\lambda = 0$ (i.e., free theory) into the following form:

$$\partial_{\theta} \phi_k(\theta) = i(\omega^2 - \xi_{\mathbf{k}}^2 + i\epsilon) \phi_k(\theta) + \eta_k(\theta) , \quad (11)$$

where the stochastic noise in this Fourier transformed basis is characterized by the following average:

$$\langle \eta_k(\theta) \eta_{k'}(\theta') \rangle_{\eta} = 2 (2\pi)^d \delta(\omega + \omega') \delta^{(d-1)}(\mathbf{k} + \mathbf{k}') \delta(\theta - \theta') . \quad (12)$$

It is a simple exercise to find an analytical solution of this linear differential equation of Eq. (11) that yields

$$\begin{aligned} \phi_k(\theta) &= \frac{1}{\partial_{\theta} - i(\omega^2 - \xi_{\mathbf{k}}^2 + i\epsilon)} \eta_k(\theta) + e^{i(\omega^2 - \xi_{\mathbf{k}}^2 + i\epsilon)\theta} \phi_k(0) \\ &= \int_0^{\theta} d\theta' e^{i(\omega^2 - \xi_{\mathbf{k}}^2 + i\epsilon)(\theta - \theta')} \eta_k(\theta') + e^{i(\omega^2 - \xi_{\mathbf{k}}^2 + i\epsilon)\theta} \phi_k(0) . \end{aligned} \quad (13)$$

The propagator is a two-point function constructed with the above ϕ_k . We should keep in mind to take the $\theta \rightarrow \infty$ limit carefully after taking the two-point function. The free Feynman propagator is immediately obtainable

through

$$\begin{aligned}
G_0(k, k') &= \lim_{\theta \rightarrow \infty} \langle \phi_k(\theta) \phi_{k'}(\theta) \rangle_\eta \\
&= (2\pi)^d \delta(\omega + \omega') \delta^{(d-1)}(\mathbf{k} + \mathbf{k}') \frac{i}{\omega^2 - \xi_{\mathbf{k}}^2 + i\epsilon} \lim_{\theta \rightarrow \infty} \left[1 - e^{2i(\omega^2 - \xi_{\mathbf{k}}^2 + i\epsilon)\theta} \right] \\
&\quad + \lim_{\theta \rightarrow \infty} e^{i(\omega^2 + \omega'^2 - \xi_{\mathbf{k}}^2 - \xi_{\mathbf{k}'}^2 + 2i\epsilon)\theta} \phi_k(0) \phi_{k'}(0). \tag{14}
\end{aligned}$$

It is important to note that we can safely take the $\theta \rightarrow \infty$ limit thanks to the presence of $\epsilon > 0$. In other words, this $i\epsilon$ term was needed in Eq. (11) for the convergence in the $\theta \rightarrow \infty$ limit and such an insertion is completely consistent with the well-known $i\epsilon$ prescription to get the Feynman (time-ordered) propagator; the second oscillatory term inside of the square brackets and the last term in Eq. (14) vanish, so that the standard expression of the free Feynman propagator emerges. The final result is independent of the choice of initial wave-functional, and this is true for any higher-order diagrams, so that we can freely adopt the initial condition as $\phi_k(0) = 0$ in the following.

For the direct real-time simulation, hence, we should keep a finite ϵ in principle and integrate the complex Langevin equation with respect to θ up to a sufficiently large value to fulfill $e^{-2\epsilon\theta} \ll 1$. However, it is impractical to realize such a condition strictly. We will come back to this point when we present our numerical results later.

2.3 Recovery of the perturbative expansion

With a finite λ of the self-interaction strength, we cannot write a full analytical solution down but still find a recursion equation or an integral equation, from which we can iteratively produce a solution of the differential equation. That is, the complex Langevin equation in momentum space translates into

$$\phi_k(\theta) = \int_0^\theta d\theta' e^{i(\omega^2 - \xi_{\mathbf{k}}^2 + i\epsilon)(\theta - \theta')} \left[\eta_k(\theta') - i\lambda \int \frac{d^d k_1 d^d k_2}{(2\pi)^{2d}} \phi_{k-k_1-k_2}(\theta') \phi_{k_1}(\theta') \phi_{k_2}(\theta') \right]. \tag{15}$$

This is a convenient expression used for the iteration that generates the expansion of $\phi_k(\theta)$ in powers of λ . The number of involved $\eta_k(\theta)$ would increase as we go to higher-order terms in the λ -expansion, which is graphically illustrated in Fig. 3 (a).

Because of the Gaussian nature of the stochastic variables (8), the η -average makes a pair of $\eta_k(\theta)$ contracted to each other. Figure 3 (b) shows an example of such contraction in the computation of $\langle \phi_k(\theta) \phi_{k'}(\theta) \rangle$. The dotted lines indicate the contracted pairs of $\eta_k(\theta)$ and the contraction results in the



Fig. 3. (a) Stochastic diagrams that represent an iterative solution of the integral equation (15). The crosses are the stochastic variables $\eta_k(\theta)$. (b) An example of contraction of the stochastic variables for the two-point function that produces a Feynman diagram of the self-energy.

lowest-order Feynman diagram of the self-energy. This procedure is readily generalized to higher-order contributions, so that the perturbative series from the ordinary quantization scheme are exactly recovered [76,86,87].

3 Numerical Simulations without Interaction

First we shall focus on the simple case without interaction; i.e., $\lambda = 0$ and for a fixed spatial momentum. The system then reduces to a 0+1 dimensional problem or a quantum mechanical problem. We reproduce the free propagator by numerical means of stochastic quantization. We explain the discretization schemes in momentum (frequency) space, and then we address the numerical results.

3.1 Discretization in frequency space

Because the boundaries at t_i and t_f are irrelevant in the $i\epsilon$ prescription, we can implicitly impose the periodic boundary condition so that we can work in frequency space (with the spatial momentum \mathbf{k} frozen). Then, we should solve Eq. (11) numerically for a given ξ , where we drop the subscript \mathbf{k} . So, the system in what follows has only t -dependence with a mass scale given by ξ ; in other words, this is a harmonic oscillator problem in quantum mechanics.

On the lattice we discretize the frequency and the mass scale as

$$\omega = \omega_{\min} \nu, \quad \xi = \omega_{\min} \mu \quad \text{with} \quad \omega_{\min} = \frac{2\pi}{N_t + 1}, \quad (16)$$

under the condition that the time t runs from $t_i = 0$ to $t_f = N_t \Delta t$ with a period $(N_t + 1)\Delta t$. We sometimes drop the time spacing Δt or express quantities in the unit of Δt . With discretization we should generate the stochastic variables

in such a way as

$$\langle \eta_\nu(\theta) \eta_{\nu'}(\theta') \rangle = \frac{2N_t}{\Delta\theta} \delta_{\nu+\nu',0} \delta_{\theta,\theta'} , \quad (17)$$

where $\Delta\theta$ is a lattice spacing in the θ direction. We note that the generation of $\eta_\nu(\theta)$ needs some caution to make $\eta(x, \theta)$ in coordinate space non-complex, which demands: $\eta_{-\nu}(\theta) = \eta_\nu^*(\theta)$. Therefore, when we generate $\eta_\nu(\theta)$, we first generate real stochastic variables $\bar{\eta}_1$ and $\bar{\eta}_2$ and then combine them as

$$\eta_\nu(\theta) = \bar{\eta}^{(1)} + i\bar{\eta}^{(2)} , \quad \eta_{-\nu}(\theta) = \bar{\eta}^{(1)} - i\bar{\eta}^{(2)} \quad (18)$$

for $\nu \neq 0$ and

$$\eta_0(\theta) = \sqrt{2} \bar{\eta}^{(1)} \quad (19)$$

for $\nu = 0$. The differential equations to be solved are thus

$$\phi_\nu(\theta + \Delta\theta) = \frac{e^{-\epsilon\Delta\theta}}{1 - i\omega_{\min}^2(\nu^2 - \mu^2)\Delta\theta} \phi_\nu(\theta) + \Delta\theta \eta_\nu(\theta) \quad (20)$$

in a resummed form. It is easy to confirm that the expansion of Eq. (20) up to the first order in $\Delta\theta$ is precisely the discretized version of the differential equation (11). We use this resummed form to enhance the numerical stability, which is improved by the fact that $\Delta\theta$ appears in the denominator.

Our goal at the present is to integrate Eq. (20) numerically and make it sure that the resulting propagator is non-vanishing for $\nu' = -\nu$ and is expected to be the analytical solution (14) or its discretized representation:

$$G(\nu, \theta) = N_t \frac{i}{\omega_{\min}^2(\nu^2 - \mu^2) + i\epsilon} \left[1 - e^{2i\omega_{\min}^2(\nu^2 - \mu^2)\theta - 2\epsilon\theta} \right]. \quad (21)$$

We note that a dimensionless mass parameter μ is not necessarily an integer, while ν is quantized corresponding to the Fourier mode under the periodic boundary condition (see Eq. (16) for definition).

Now let us consider the propagator for a specific choice of parameters; $\mu = 64$ and $N_t = 256$. We show the imaginary part of $G(\nu, \theta)$ from our numerical results in Fig. 4; we take the ensemble average over 1000 independent runs with $\Delta\theta = 10^{-2}$ and $\epsilon = 10^{-2}$. We can see that the results at $\theta = 10$ (left of Fig. 4) turns out to be quite consistent with the analytical expectation from Eq. (21). We emphasize that our numerical results in the left of Fig. 4 even reproduce the fine structure of oscillation term, $e^{2i\omega_{\min}^2\nu^2\theta}$, because the damping factor $e^{-2\epsilon\theta} \simeq 0.82$ is not small. Therefore we should take either a larger ϵ or a larger θ for better convergence. If ϵ gets larger, however, the propagator poles would become obscure. If we continue our simulation till larger θ , the numerical results suffer from severe fluctuations as shown in the right of Fig. 4 (which is an example at $\theta = 50$). These rough results are caused not by numerical instability but merely by statistical problem. As we evolve the field value with increasing θ , we accumulate all contributions from $\eta_\nu(\theta)$ at each step of θ . This

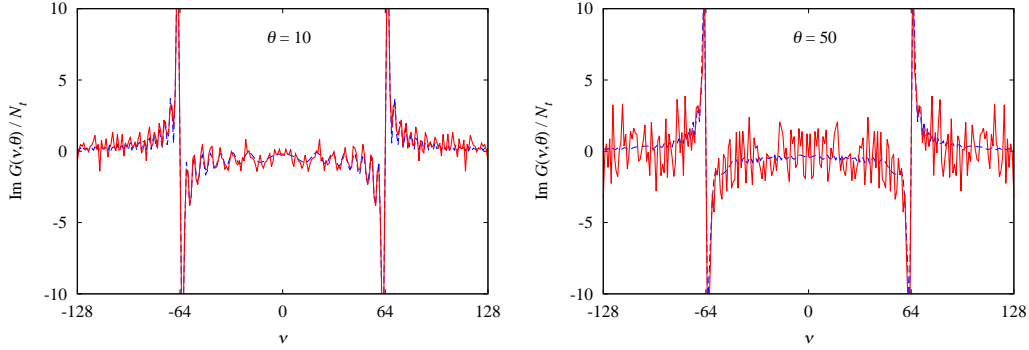


Fig. 4. Numerical solution for the free propagator with the ensemble average over 1000 independent runs with $\epsilon = 10^{-2}$ at $\theta = 10$ (left) and $\theta = 50$ (right). We choose $\Delta\theta = 10^{-2}$ and $\mu = 64$.

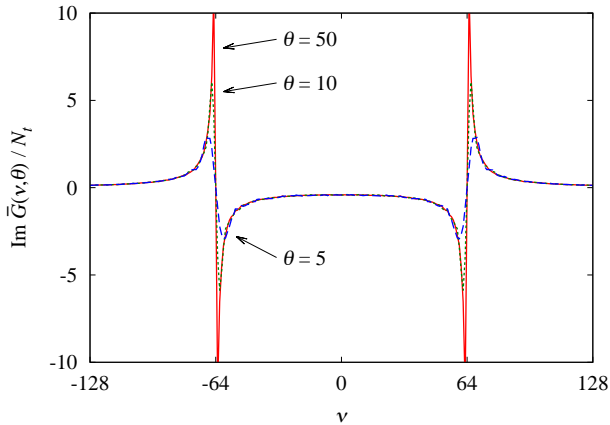


Fig. 5. Numerical results for the θ -averaged propagator with the ensemble average still taken over 1000 independent runs. Dashed, dotted, and solid curves represent the results at $\theta = 5$, 10, and 50, respectively. We choose $\Delta\theta = 10^{-2}$ and $\mu = 64$ again.

means that we need to prepare more independent runs with increasing $\theta/\Delta\theta$ to get convergent results. It is therefore a time-consuming task to evolve the system up to $\theta = 10^6$ to suppress unwanted oscillations.

We can reduce the computational cost by averaging out to get rid of the oscillatory part out from the vacuum contribution. That is, we see that the oscillatory part quickly disappears once we take a θ -average that is defined by

$$\overline{\langle \mathcal{O}[\phi(x, \theta)] \rangle_\eta} \equiv \frac{1}{\theta} \int_0^\theta d\theta \langle \mathcal{O}[\phi(x, \theta)] \rangle_\eta, \quad (22)$$

which is supposed to coincide with the correct expectation value for a large value of θ if the unnecessary terms killed by a finite ϵ are always accompanied by θ -oscillation. This is a common practice and most of numerical works in

the literature [72] makes use of this trick. Nevertheless, strictly speaking, it is a non-trivial question whether this procedure of taking the θ -average is always harmless not affecting the physical answer for any operators. To the best of our knowledge we do not have a general proof but we have performed explicit calculations for the one-loop self-energy to confirm that Eq. (22) gives the correct answer, which is explained in details in Appendix A.

The example in Fig. 4 evidently indicates the necessity of taking the θ -average to acquire converging results within reasonable machine time. Now we make use of the θ -averaging procedure of Eq. (22) to compute the propagator, which is plotted in Fig. 5. It is obvious at a glance that the simulation quickly converges to the smooth curve of the free propagator already around $\theta \sim 10$.

4 Inclusion of Interaction Effects

Let us continue our discussions with interaction effects using the same quantum mechanical (0+1 dimensional) example where no ultraviolet divergence appears and thus the theoretical setup is clean. The Langevin equation with $\lambda \neq 0$ reads in frequency space:

$$\partial_\theta \phi_\nu(\theta) = i(\omega^2 - \xi^2 + i\epsilon) \phi_\nu(\theta) - \frac{i\lambda}{N_t^2} \sum_{\nu_1, \nu_2} \phi_{\nu_1}(\theta) \phi_{\nu_2}(\theta) \phi_{\nu-\nu_1-\nu_2}(\theta) + \eta_\nu(\theta). \quad (23)$$

The question is how to discretize the above differential equation avoiding numerical instability. If we simply add the interaction term on top of our procedure in the previous section, numerical instability badly grows up for $\Delta\theta = 10^{-2}$ (but a smaller $\Delta\theta$ like 10^{-5} can stabilize the simulation).

4.1 Exact and approximated results

In this simple system we can find the “exact” answer by diagonalizing the Hamiltonian using the harmonic oscillator bases, which is elucidated in details in Appendix B. Interestingly, in this case, the mean-field approximation or the Hartree approximation would lead to results surprisingly close to the exact answer. In this approximation the interaction effects are assumed to be all renormalized in the effective mass. In the one-loop level the self-energy in the continuum theory (which is already a good approximation in our setup with $N_t = 256$) is found as

$$\Pi = i(-i6\lambda) \cdot \frac{1}{2} \int \frac{d\omega}{2\pi} \frac{i}{\omega^2 - \xi^2 + i\epsilon} = \frac{3\lambda}{2\xi}. \quad (24)$$

We note that this one-dimensional integration results in a finite number. Hence, the effective mass should be shifted by $M^2 = \xi^2 + \Pi$ at the one-loop order. In the mean-field resummation, the one-loop tadpole diagrams are all taken into account through the self-consistency condition or the gap equation,

$$M^2 = \xi^2 + \frac{3\lambda}{2M}, \quad (25)$$

in which the bare mass in Eq. (24) is replaced with the effective mass M . We can write the analytical solution of the gap equation down as

$$M = \left(\frac{3\lambda}{4} + \sqrt{\frac{9\lambda^2}{16} - \frac{\xi^6}{27}} \right)^{1/3} + \left(\frac{3\lambda}{4} - \sqrt{\frac{9\lambda^2}{16} - \frac{\xi^6}{27}} \right)^{1/3}. \quad (26)$$

We plot the dimensionless M/ξ as a function of the dimensionless coupling λ/ξ^3 in Fig. 6. From this we can deduce how much the effective mass M is enhanced from the bare mass ξ . For example, if we use $\lambda = 0.5$ and $\xi = \omega_{\min} \cdot \mu$ with $\mu = 24$ and 64 , the dimensionless coupling is $\lambda/\xi^3 \simeq 2.48$ and 0.13 . Then, multiplying the enhancement factor inferred from Fig. 6, we can get the mean-field masses as $M = \omega_{\min} \cdot \mu'$ with $\mu' \approx 42.3$ and 69.5 , respectively. We will confirm these estimates soon later.

We here would like to draw an attention to the fact that the mean-field results are amazingly close to the numerically exact answer. This nice agreement is attributed to the behavior of the full numerical solution of this anharmonic oscillator problem; the residue of the propagator hardly deviates from the unity and the imaginary part in the self-energy does not arise due to the phase space limitation. In other words, in the language of the 0+1 dimensional field theory, the wave-function renormalization is negligibly small in this particular case.

4.2 Numerical results with the full interaction

We can take account of the self-interaction terms by adding them to Eq. (20) as they appear in Eq. (23). However, this straightforward implementation is not very stable for a long time run. We find that it would be much advantageous to add the interaction terms in original t -space by taking the Fourier transformation back. The interaction is local then, while many non-local terms are involved in ω -space as in Eq. (23).

For concrete procedures of the updates, we first prepare $\phi(t, \theta)$ and its Fourier transform $\phi_\nu(\theta)$. Then we calculate the difference from the kinetic term in ω -space as

$$\phi_\nu(\theta) + \delta\phi_\nu(\theta) = \frac{e^{-\epsilon\Delta\theta}}{1 - i\omega_{\min}^2(\nu^2 - \mu^2)\Delta\theta} \phi_\nu(\theta). \quad (27)$$

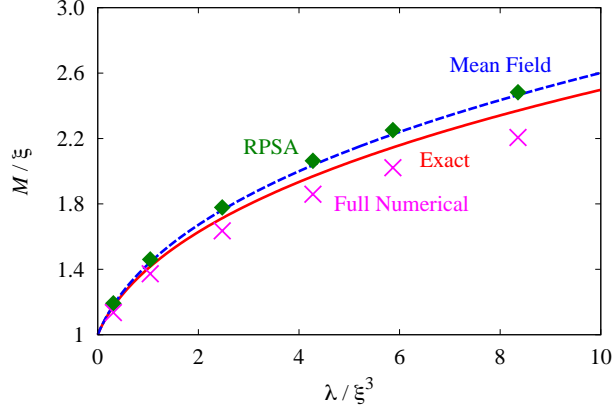


Fig. 6. Effective mass, M , as a function of the coupling λ in the unit of ξ . The solid curve represents the exact answer by diagonalization of the Hamiltonian, the dashed one is the self-consistent solution (26). The filled diamonds represent the results from the restricted phase-space approximation we are proposing, while the crosses are the full numerical results without truncation; see the text for more explanations.

Also we calculate the difference coming from the interaction terms in t space as

$$\begin{aligned} \phi(t, \theta) + \delta\phi(t, \theta) &= \phi(t, \theta) - i\lambda\phi^3(t, \theta)\Delta\theta + \eta(t, \theta)\Delta\theta \\ &\approx \frac{\phi(t, \theta)}{\sqrt{1 + 2i\lambda\phi^2(t, \theta)\Delta\theta}} + \eta(t, \theta)\Delta\theta. \end{aligned} \quad (28)$$

The numerical instability occurs when $\phi^3(t, \theta)\Delta\theta$ happens to take a large number. The above resummed form is convenient to avoid such a problem of instability. We make a remark that this special form solves $\partial\phi/\partial\Delta\theta = -i\lambda\phi^3$. Thanks to the stability we can adopt $\Delta\theta = 10^{-2}$ below.

In this way we can calculate the propagator with full interaction effects for $\lambda = 0.5$ and various values of ξ (or μ). Figure 7 is an example of our simulation for $\mu = 64$. Because there is no allowed phase space in spatial zero-dimension, the physical width should be vanishing even in the fully interacting case. Our simulation results, however, exhibit some unphysical width as seen in Fig. 7, while we can get reasonable results if we force ϵ to be as large as ~ 1 . When ϵ becomes 0.5 or smaller, the full results start differing from the expected exact ones: not only the unphysical width appears but the propagator residue is also rotated with some complex number, which can be fitted well by

$$G(\omega) = \frac{iA}{\omega^2 - M^2 + i\Gamma}. \quad (29)$$

As we described, as long as $\epsilon \gtrsim 1$, we find $A \sim 1$ and $\Gamma \sim \epsilon$. For smaller ϵ about 10^{-2} , the residue A turns out to be $\sim -2i$ and Γ is of order of the unity. We have also reconfirmed this behavior using the upper of Eq. (28) directly

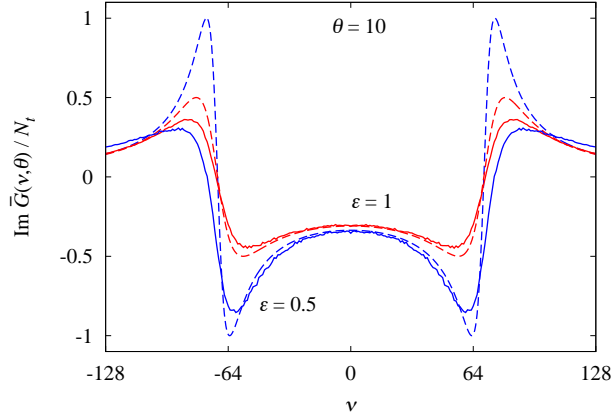


Fig. 7. Numerical results (by solid curves) for the θ -averaged full propagators with $\mu = 64$ for $\epsilon = 0.5$ and 1.0 at $\theta = 10$ with the ensemble average taken over 1000 independent runs. The interaction strength is chosen to be $\lambda = 0.5$. The dashed curves represent the (free) propagators with the effective mass $M = 69.5\omega_{\min}$ (mean-field value) and corresponding ϵ .

with $\Delta\theta = 10^{-5}$, and so we can say that unphysical A and Γ for small ϵ are induced not only under the resummation of Eq. (28). There seems to be an unphysical fixed-point in the theory itself.

Although the shape of (the imaginary-part of) the propagator has funny modifications with A and Γ , the effective mass M turns out to be still close to the right value. We have performed the fitting between our numerical results and the ansatz of Eq. (29) for $\lambda = 0.5$ with $\mu = 48, 32, 24, 20, 18, 16$. The global behavior of M obtained from the fit with the full numerical results is fairly consistent with the exact answer as seen in Fig. 6. We note that these are results for a choice of $\epsilon = 0.1$, but other values of ϵ would make only a tiny quantitative difference.

4.3 Unphysical fixed-point

The transparent method to figure the flow pattern out with changing θ is to find the fixed-points using the Fokker-Planck equation [88] which describes the equivalent dynamics as the Langevin equation does. One can prove that the probability function, $P[\phi_R, \phi_I]$, should obey the following differential equation

(see Ref. [46] for derivations and also references therein for further details):

$$\begin{aligned}
\frac{\partial P}{\partial \theta} &= \int \frac{d\omega}{2\pi} \left[\frac{\delta}{\delta \phi_{\text{R}}(\omega)} \left(\text{Im} \frac{\delta S}{\delta \phi(-\omega)} + \frac{\delta}{\delta \phi_{\text{R}}(-\omega)} \right) - \frac{\delta}{\delta \phi_{\text{I}}(\omega)} \text{Re} \frac{\delta S}{\delta \phi(-\omega)} \right] P \\
&= \int \frac{d\omega}{2\pi} \left\{ 2\pi \delta(0) \cdot 2\epsilon - 12\lambda \int \frac{d\omega'}{2\pi} \phi'_{\text{R}} \phi'_{\text{I}} + \frac{\delta^2}{\delta \phi_{\text{R}}^2} + \epsilon \left(\phi_{\text{R}} \frac{\delta}{\delta \phi_{\text{R}}} + \phi_{\text{I}} \frac{\delta}{\delta \phi_{\text{I}}} \right) \right. \\
&\quad + (\omega^2 - m^2) \left(\phi_{\text{I}} \frac{\delta}{\delta \phi_{\text{R}}} - \phi_{\text{R}} \frac{\delta}{\delta \phi_{\text{I}}} \right) - \lambda \int \frac{d\omega' d\omega''}{(2\pi)^2} (3\phi_{\text{R}}''' \phi'_{\text{R}} \phi''_{\text{I}} - \phi_{\text{I}}''' \phi'_{\text{I}} \phi''_{\text{R}}) \frac{\delta}{\delta \phi_{\text{R}}} \\
&\quad \left. - \lambda \int \frac{d^2 \omega' \omega''}{(2\pi)^2} (3\phi_{\text{R}}''' \phi'_{\text{I}} \phi''_{\text{I}} - \phi_{\text{R}}''' \phi'_{\text{R}} \phi''_{\text{R}}) \frac{\delta}{\delta \phi_{\text{I}}} \right\} P, \tag{30}
\end{aligned}$$

where we shortened our notation by writing ϕ'_{R} and ϕ'_{I} to denote fields with the frequency ω' , ϕ''_{R} and ϕ''_{I} with ω'' , and ϕ'''_{R} and ϕ'''_{I} with $\omega - \omega' - \omega''$, with an exception that $\phi'_{\text{R}} \phi'_{\text{I}}$ in the first line represents $\phi_{\text{R}}(-\omega') \phi_{\text{I}}(\omega')$. In the end of the $\theta \rightarrow \infty$ limit, $P[\phi_{\text{R}}, \phi_{\text{I}}; \theta]$ should converge to an asymptotic form at the fixed-point. In the free case with $\lambda = 0$ it is easy to confirm that the following probability function:

$$P[\phi_{\text{R}}, \phi_{\text{I}}] = N \exp \left[-\epsilon \int \frac{d\omega}{2\pi} (\phi_{\text{R}}, \phi_{\text{I}}) \begin{pmatrix} 1 & -\frac{\epsilon}{\omega^2 - m^2} \\ -\frac{\epsilon}{\omega^2 - m^2} & 1 + \frac{2\epsilon^2}{(\omega^2 - m^2)^2} \end{pmatrix} \begin{pmatrix} \phi_{\text{R}} \\ \phi_{\text{I}} \end{pmatrix} \right] \tag{31}$$

solves $\partial P / \partial \theta = 0$. Because we have numerically found in the previous subsection that our results support a fitting ansatz of Eq. (29), we should be able to perform fixed-point analysis in the parameter space spanned by A , M , and Γ . In this way, from $\partial P / \partial \theta = 0$, we can derive equations for these ‘‘variational parameters’’ that play the role of the gap equations. The full analysis has turned out to be quite complicated and we would like to leave detailed descriptions for a separate paper.

The Fokker-Planck equation (30) is, however, sufficiently useful for us to understand why our numerical results in Sec. 4.2 tend to fall into a wrong branch of A and Γ . In the free case we immediately see from Eqs. (30) and (31) that the first term involving 2ϵ is exactly canceled by $\delta^2 / \delta \phi_{\text{R}}^2$ hitting on the exponential part of Eq. (31). Once we modify $P[\phi_{\text{R}}, \phi_{\text{I}}]$ to allow for a complex residue $A = |A|e^{i\alpha}$ and a width Γ , the corresponding probability function has a ϕ_{R}^2 -component with a mixture of $\Gamma \cos \alpha$ and $(\omega^2 - m^2) \sin \alpha$. Thus, $\delta^2 / \delta \phi_{\text{R}}^2$ would generate a very singular term proportional to $\int d\omega \omega^2 \sin \alpha$, so that $\partial P / \partial \theta = 0$ is easily achieved by an appropriate (but unphysical) choice of $\alpha \neq 0$ because its coefficient $\int d\omega \omega^2$ is overwhelming. This is an intuitive explanation of how an unphysical fixed-point cannot be avoidable with a complex residue of the propagator, as we numerically observed in the previous subsection.

As long as such an unphysical fixed-point is well separated from the physical trajectories, the numerical simulation can correctly identify the physical fixed-

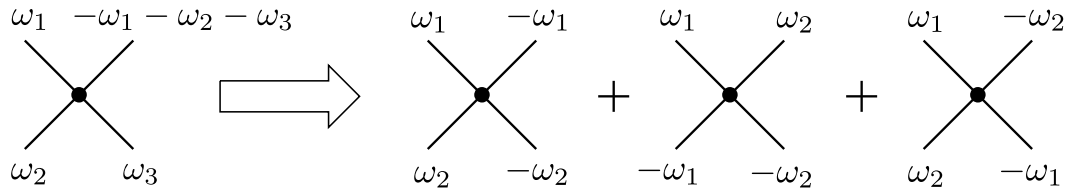


Fig. 8. Schematic illustration for the RPSA that we propose in this paper. The phase space associated with scattering is restricted to the limit of small angle (zero momentum transfer) in the s -, t -, and u -channels. This treatment does not damage the essential features of real-time dynamics and even becomes exact in special models such as the large N limit of $O(N)$ scalar model.

point, which is the case in the free theory. The flow structure around the fixed-points or attractors becomes highly involved for general $\lambda \neq 0$, and when the physical region is contaminated by the unphysical fixed-point, the simulation is stuck with pathological behavior (a part of which might be cured by the change of variables as discussed in Ref. [89]). A more complete study will be reported elsewhere (including the explicit check of the locality and the Dyson equations; see Refs. [90,91]).

4.4 Restricted phase-space approximation (RPSA)

Here we would propose a “restricted phase-space approximation” (RPSA) that is defined by the following truncation in the interaction terms:

$$\sum_{\nu_1, \nu_2} \phi_{\nu_1}(\theta) \phi_{\nu_2}(\theta) \phi_{\nu-\nu_1-\nu_2}(\theta) = 3 \sum_{\nu_1} \phi_{-\nu_1}(\theta) \phi_{\nu_1}(\theta) \phi_{\nu}(\theta) + (\text{others}) . \quad (32)$$

In the RPSA we discard terms referred to as “others” in the above. We emphasize that this truncation should not damage the essential features of real-time dynamics; in fact, if we work in the $O(N)$ scalar theory and take the limit of $N \rightarrow \infty$, only the daisy diagrams remain in the leading order of the $1/N$ expansion and discarded terms are all dropped off. Therefore, the RPSA becomes exact in this special case. We present Fig. 8 for a schematic illustration of the RPSA for the ϕ^4 interaction.

In this prescription of the RPSA we can express the differential equation as if it were a free-theory problem with a renormalized mass-like term; i.e.,

$$\phi_{\nu}(\theta + \Delta\theta) = \frac{e^{-\epsilon\Delta\theta}}{1 - e^{i(\omega^2 - \bar{\xi}^2)}} \phi_{\nu}(\theta) + \eta_{\nu}(\theta) , \quad (33)$$

$$\bar{\xi}^2 \equiv \xi^2 + \frac{3\lambda}{N_t^2} \sum_{\nu_1} \phi_{-\nu_1}(\theta) \phi_{\nu_1}(\theta) . \quad (34)$$

It should be mentioned that $\bar{\xi}^2$ is not a mass but it still involves interactions.

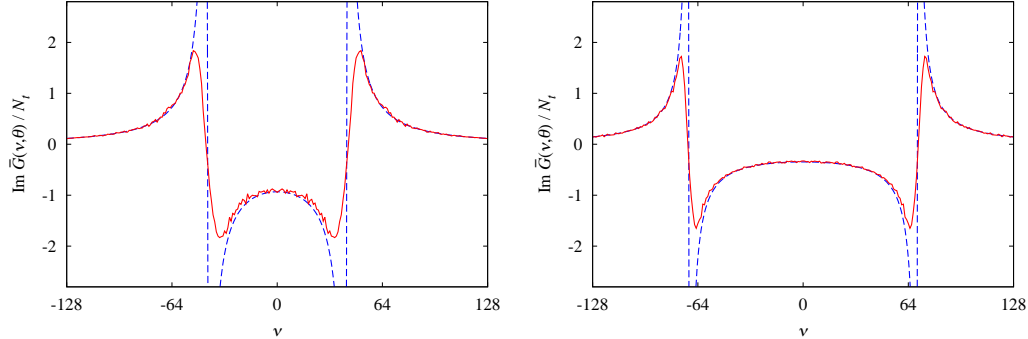


Fig. 9. Numerical results (by solid curves) for the θ -averaged propagator at $\theta = 5$ with the ensemble average taken over 1000 independent runs. We adopt $\xi = 24$ (left) and $\xi = 64$ (right), respectively. The interaction strength is chosen to be $\lambda = 0.5$. The dashed curves represent the mean-field propagator.

So, the RPSA is not a mean-field approximation and $\bar{\xi}$ is not a mean-field mass. The point is that we can treat $\bar{\xi}$ in the same way as the mass in the numerical procedure. This implies that the numerical simulation is stable even with non-zero λ as long as it is stable for a free theory.

Figure 9 shows our numerical results in the RPSA for the propagator with interaction $\lambda = 0.5$ and the bare mass $\mu = 24$ (left) and $\mu = 64$ (right), respectively. In view of these results we can make sure that unphysical width is suppressed, and indeed, the peak becomes sharper if we extend the simulation till a further larger value of θ . So, we here manage to avoid the unphysical fixed-point.

It is quite impressive that our numerical results agree well with the mean-field propagator in which the mean-field masses are plugged; namely, $\mu' \approx 42.3$ for $\mu = 24$ and $\mu' = 69.5$ for $\mu = 64$ as shown by dashed curves in Fig. 9.

Let us make this kind of comparison more quantitative. We can fit the numerical results using the parametrization of Eq. (29). In this case of RPSA we find that A is always close to the unity and Γ is as small as ϵ once we continue the simulation up to a sufficiently large θ . Then, we deduce the effective masses M corresponding to $\mu = 48, 32, 24, 20, 18, 16$ and put crosses on Fig. 6. Surprisingly, the resultant M turns out to be on top of the mean-field prediction, though the RPSA is not really equivalent to the mean-field approximation.

5 Closed-time Path Formalism

Now we have understood how we can correctly reproduce the free propagator in frequency space with help of the $i\epsilon$ prescription. In this section let us briefly sketch how we can apply the closed-time path formalism to compute

the vacuum expectation value directly in a form of Eq. (5) not relying on the $i\epsilon$ prescription, which would be extended to more general non-equilibrium environments.

For simplicity we limit ourselves only to the free theory because we can carry out analytical evaluations using an explicit form of the vacuum wave-function:

$$\Psi_0[\phi] \equiv \langle \phi | \Omega \rangle = \left(\frac{m}{\pi} \right)^{1/4} \exp\left(-\frac{m}{2} \phi^2 \right). \quad (35)$$

We shall see the recovery of the free propagator in what follows. We compute the two-point function with inserting the complete sets; $\int d\phi_i |\phi_i\rangle \langle \phi_i|$ and $\int d\phi'_i |\phi'_i\rangle \langle \phi'_i|$ as

$$\langle \Omega | \phi(t_f) \phi(t_i) | \Omega \rangle = \sqrt{\frac{m}{\pi}} \int d\phi_i d\phi'_i e^{-m(\phi_i^2 + \phi_i'^2)/2} \phi_i \langle \phi'_i | e^{-iH(t_i - t_f)} \phi e^{-iH(t_f - t_i)} | \phi_i \rangle. \quad (36)$$

Then, using the Fock space bases, we can write the matrix element appearing in the above expression as

$$\begin{aligned} & \sum_{n, n'} \langle \phi'_i | n' \rangle \langle n' | e^{-iH(t_i - t_f)} \phi e^{-iH(t_f - t_i)} | n \rangle \langle n | \phi_i \rangle \\ &= e^{-im(t_f - t_i)} \sum_n \langle \phi'_i | n - 1 \rangle \langle n - 1 | \phi | n \rangle \langle n | \phi_i \rangle + e^{im(t_f - t_i)} \sum_n \langle \phi'_i | n + 1 \rangle \langle n + 1 | \phi | n \rangle \langle n | \phi_i \rangle \\ &= \cos[m(t_f - t_i)] \phi'_i \delta(\phi_i - \phi'_i) - i \sin[m(t_f - t_i)] \frac{d}{m d\phi'_i} \delta(\phi_i - \phi'_i). \end{aligned} \quad (37)$$

We can readily reach the final answer as follows:

$$\langle \Omega | \phi(t_f) \phi(t_i) | \Omega \rangle = e^{-im(t_f - t_i)} \sqrt{\frac{m}{\pi}} \int d\phi_i \phi_i^2 e^{-m\phi_i^2} = \frac{1}{2m} e^{-im(t_f - t_i)}. \quad (38)$$

This is an almost trivial example; nevertheless, it is far from trivial to understand how the CTP formalism in stochastic quantization works out to realize this simple propagator. In the CTP formalism the matrix element appearing in Eq. (36) is put into a form of the functional integral (or the path integral in our one-dimensional example) that is written as

$$\begin{aligned} \langle \phi'_i | e^{-iH(t_i - t_f)} \phi e^{-iH(t_f - t_i)} | \phi_i \rangle &= \int d\phi_f d\phi'_f \int_{\phi'_f \rightarrow \phi'_i} \mathcal{D}\phi e^{iS} \langle \phi'_f | \phi | \phi_f \rangle \int_{\phi_i \rightarrow \phi_f} \mathcal{D}\phi e^{iS} \\ &= \int d\phi_f \phi_f \oint_{\phi_i \rightarrow \phi_f \rightarrow \phi'_i} \mathcal{D}\phi e^{iS}. \end{aligned} \quad (39)$$

Here $\int_{\phi_i \rightarrow \phi_f}$ represents the path integral with a boundary with the initial condition $\phi = \phi_i$ at $t = t_i$ and the final condition $\phi = \phi_f$ at $t = t_f$, etc. The standard knowledge on the path integral representation of quantum mechanics tells us that this path integral part is nothing but the Feynman kernel whose explicit

form is

$$\int_{\phi_i \rightarrow \phi_f} \mathcal{D}\phi e^{iS} = \sqrt{\frac{m}{2\pi i \sin[m(t_f - t_i)]}} \times \exp\left\{\frac{im}{2 \sin[m(t_f - t_i)]} \left[(\phi_i^2 + \phi_f^2) \cos[m(t_f - t_i)] - 2\phi_i \phi_f \right]\right\}, \quad (40)$$

for the harmonic oscillatory (see Ref. [92] for a well-known textbook). We can rederive the matrix element (37) using the above Feynman kernel (40). It is a bit tedious calculation, but quite instructive, so we summarize the key equations of the derivation below.

From the Feynman kernel (40) the path integral along the closed contour is found to take:

$$\oint_{\phi_i \rightarrow \phi_f \rightarrow \phi_i} \mathcal{D}\phi e^{iS} = \frac{m}{2\pi \sin[m(t_f - t_i)]} \times \exp\left\{\frac{im}{2 \sin[m(t_f - t_i)]} \left[(\phi_i^2 - \phi_i'^2) \cos[m(t_f - t_i)] - 2(\phi_i - \phi_i')\phi_f \right]\right\}. \quad (41)$$

Then, we can perform the integration with respect to ϕ_f that picks up the following part from the whole expression:

$$\int d\phi_f \phi_f \exp\left\{\frac{-im(\phi_i - \phi_i')}{\sin[m(t_f - t_i)]} \phi_f\right\} = \frac{\sin^2[m(t_f - t_i)]}{im^2} \frac{d}{d\phi_i'} 2\pi \delta(\phi_i - \phi_i'). \quad (42)$$

Because ϕ_i' is an integration variable in the convolution with the initial wave function, we can move the derivative using the integration by part to reach:

$$\begin{aligned} \int d\phi_f \phi_f \operatorname{Re} \oint_{\phi_i \rightarrow \phi_f \rightarrow \phi_i'} \mathcal{D}\phi e^{iS} &= \frac{m}{2\pi \sin[m(t_f - t_i)]} \\ &\times \frac{im}{\sin[m(t_f - t_i)]} \cos[m(t_f - t_i)] \phi_i' \cdot \frac{\sin^2[m(t_f - t_i)]}{im^2} 2\pi \delta(\phi_i - \phi_i') \\ &= \cos[m(t_f - t_i)] \phi_i \delta(\phi_i - \phi_i'). \end{aligned} \quad (43)$$

The ϕ_i' derivative acts also on the wave function, so that it yields the imaginary part of Eq. (37) in the same way. Then, we can explicitly see that we surely reproduce the matrix element of Eq. (37) and thus Eq. (38) as well.

This is how the CTP formalism works analytically to describe the time evolution. We focused on the vacuum expectation value in a free theory, but the generalization is not difficult. Even for more complicated operators with interaction turned on, one can understand that the most fundamental building block for the formalism is still the matrix element (37) of the free propagation; therefore, we will concentrate on this quantity in our numerical analysis below.

Just for the test purpose of the CTP formalism, we shall fix $\phi_i = \phi'_i$ in the beginning and then calculate the expectation value of $\phi(t_f)$ to pick up the diagonal component of Eq. (37). It should be mentioned that in stochastic quantization we cannot directly calculate the amplitude such as the Feynman kernel but it is always an “expectation value” of some operator that we can estimate. Thus, with a given boundary condition, $\phi_i = \phi'_i$, if we compute the η -average of $\phi(t_f)$, it should be interpreted as

$$\frac{\langle \phi_i | e^{-iH(t_i-t_f)} \phi e^{-iH(t_f-t_i)} | \phi_i \rangle}{\langle \phi_i | \phi_i \rangle} = \phi_i \cos[m(t_f - t_i)]. \quad (44)$$

We note that $\delta(0)$ cancels in this ratio. This is the quantity that we wish to reproduce in the following numerical test of stochastic quantization. That is, we will compute the left-hand side of Eq. (44) to check if the numerical results coincide with the right-hand side. One might have a feeling that such a numerical calculation only to have $\cos[m(t_f - t_i)]$ should have no problem. From the point of view of practical numerical procedures, however, it is not really so because the time evolution emerges in a finite extent of time between t_i and t_f , and so the boundary condition at t_f is also necessary for the numerical derivative there. The CTP formalism provides us with a natural solution as we will see soon later.

We discretize in t -space and replace the derivatives with appropriate finite differences. As is well known in the numerical analysis of the diffusion equation, a naïve replacement called the Euler method is not stable depending on the ratio of $\Delta\theta$ and Δt [93]. It is a textbook knowledge how to improve the numerical stability; in the implicit method a part of $\phi(t, \theta)$ and $\phi(t \pm \Delta t, \theta)$ are replaced with $\phi(t, \theta + \Delta\theta)$ and $\phi(t \pm \Delta t, \theta + \Delta\theta)$, which significantly enhances the stability. Here, let us adopt a simple algorithm; i.e., the half implicit method aka Crank-Nicolson method, which is easier in our case than another common choice; that is, the adaptive stepsize method [94]. In this half implicit method the Laplacian is concretely implemented via

$$D_{2N_t+1} \begin{pmatrix} \phi(t_i, \theta + \Delta\theta) \\ \phi(t_i + \Delta t, \theta + \Delta\theta) \\ \vdots \\ \phi(t_f, \theta + \Delta\theta) \end{pmatrix} = [D_{2N_t+1}^* - i\Delta\theta\xi^2 I] \begin{pmatrix} \phi(t_i, \theta) \\ \phi(t_i + \Delta t, \theta) \\ \vdots \\ \phi(t_f, \theta) \end{pmatrix} + \Delta\theta \begin{pmatrix} \eta(t_i, \theta) \\ \eta(t_i + \Delta t, \theta) \\ \vdots \\ \eta(t_f, \theta) \end{pmatrix}. \quad (45)$$

Hereafter, we rescale all variables such as ξ to make them dimensionless by multiplying a proper power of Δt ; i.e., we measure all quantities in the unit of Δt . Here D_{2N_t+1} represents the derivative (Laplacian) matrix. Including the forward and the backward paths between t_i and t_f discretized with N_t sites, D_{2N_t+1} is a $(2N_t + 1) \times (2N_t + 1)$ matrix on the closed path. Taking account of the change of the sign of Δt in the backward direction, we can write the

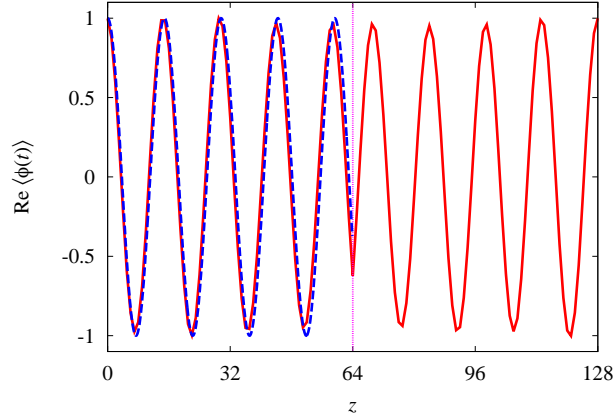


Fig. 10. Simple demonstration of the CTP formalism; the field profile at $\theta = 500$. The closed path is unfolded with t replaced with z (see Fig. 2) to separate the forward path ($t = t_i \rightarrow t_f$) and the backward path ($t = t_f \rightarrow t_i$) where $t_f = 64$. The ensemble average is taken over 100 runs. The dashed curve represents $\phi_i \cos(mt)$.

discretized matrix down as

$$D_{2N_t+1} = \left(\begin{array}{c|c|c} D_{N_t} & & \mathbf{0} \\ \hline & -\frac{1}{2}\alpha & \\ \hline -\frac{1}{2}\alpha & 1 & \frac{1}{2}\alpha \\ \hline \mathbf{0} & \frac{1}{2}\alpha & D_{N_t}^* \end{array} \right), \quad (46)$$

where D_{N_t} represents the $N_t \times N_t$ sub-matrix defined as

$$D_{N_t} = \begin{pmatrix} 1 + \alpha & -\frac{1}{2}\alpha & & \mathbf{0} \\ -\frac{1}{2}\alpha & 1 + \alpha & -\frac{1}{2}\alpha & \\ & \ddots & \ddots & \ddots \\ \mathbf{0} & & -\frac{1}{2}\alpha & 1 + \alpha \end{pmatrix}. \quad (47)$$

We note that α is a pure-imaginary number given by $\alpha \equiv -i\Delta\theta/\Delta t^2$. What we need is the field value at the next step, $\theta + \Delta\theta$, and thus, we can solve them by applying $D_{2N_t+1}^{-1}$ on the both sides of Eq. (45).

We present our numerical results in Fig. 10 in which the time axis is unfolded from t to z ; we should interpret $z > t_f$ as $t = z - t_f$ on the backward path returning to t_i . For the results in Fig. 10 we choose $N_t = 64$ and so z runs from 0 to 128. The initial value is chosen to be $\phi_i = \phi'_i = 1$. The oscillation period is determined by the mass parameter ξ that is now fixed to be $\xi = 4.25$, which

means that 4.25 periods should appear between $t = 0$ and 63 as is indeed the case in Fig. 10. Because the matrix (46) has a special point at $t = t_f$, the derivative jumps there, so that the time evolution is reflected from the forward to the backward direction correctly. This is in fact the reason why the backward path is absolutely needed in the CTP formalism. Although we need the physical information only within the time range, $z = 0 \sim 64$, it is impossible to get it without the duplication from the time range $z = 64 \sim 128$.

Now that the most essential part of the dynamical description, i.e., Eq. (37) is nicely reproduced, the vacuum expectation value can be immediately derived from the convolution with the wave function. We do not show this part of the numerical results because the calculation is just a Gaussian integral. It is quite conceivable that the same machinery should be effective even when the initial state is not a simple Gaussian function like Eq. (35) (which is adopted here to yield the vacuum expectation value and was also assumed in non-equilibrium study in Ref. [73] just for brevity). For the extensive investigation of non-equilibrium phenomena using the CTP formalism in stochastic quantization, we will report our results in follow-up publication. We shall close our present discussions with this simple but clear-cut demonstration of the strength of the CTP formalism.

6 Summary and future extensions

We have investigated the feasibility of stochastic quantization in a simple system of 0+1 dimensional scalar theory or a quantum mechanical system. We focus on the vacuum properties with the $i\epsilon$ prescription and have tested the convergence. As long as the vacuum properties are concerned, the boundary condition in time is irrelevant thanks to the $i\epsilon$ prescription, and we can work in momentum-frequency space (that corresponds to the periodic boundary condition). We find it easier to enhance the numerical stability in frequency space and have succeeded in performing the stable simulation taking account of interaction effects.

Because we can alternatively solve 0+1 dimensional ϕ^4 theory or an anharmonic oscillator problem in quantum mechanics by diagonalization of the Hamiltonian with sufficiently large number of bases, we have made a quantitative comparison between the numerically exact results and our results from stochastic quantization. Although the pole of the propagator or the effective mass behaves consistently with the correct answer, there are unphysical width and residue appearing in the propagator, which indicates that the numerical solution of stochastic quantization falls into some unphysical fixed-point. We could give an argument on the existence of such unphysical fixed-point using the alternative representation using the Fokker-Planck equation. We propose

a prescription to overcome this problem; that is, the restricted phase-space approximation (RPSA) that would be exact in the $O(N \rightarrow \infty)$ theory. In the RPSA the interaction is modified in such a way that the allowed phase space is limited. In frequency space, in particular, the RPSA makes it possible to implement the interaction in a semi-local manner and to improve the numerical stability drastically. Our comparison has revealed that the RPSA results are remarkably close to the mean-field estimate of the effective mass, which are also close to the full exact answer. It should be an interesting future work to test the further potential of the RPSA in 3+1 dimensional systems. We have performed some preliminary simulations and it is likely that the stable simulation is feasible enough to have physically meaningful results.

It is not yet clear if the RPSA can describe general non-equilibrium phenomena; the RPSA becomes most effective when formulated in momentum-frequency space but the periodicity can be lost for problems out of the vacuum state. Nevertheless, it is expected to work near the thermal equilibrium; for example, we can apply our real-time method to compute the spectral functions at finite temperature. Also, the particle production problem under time-dependent external fields would be an ideal setup to test the merit of the RPSA; this is a phenomenon associated with the change of the “vacuum” induced by external fields, which we can investigate not losing the advantage of the $i\epsilon$ prescription [70].

On the formal level, as we already mentioned, the RPSA would become exact in the large- N limit. It should be theoretically an intriguing question to formulate the $O(N \rightarrow \infty)$ theory with stochastic quantization, which may provide us with a hint to represent the theory in higher dimensions (with an extra coordinate of the fictitious time added). It would be conceivable that stochastic approaches could be useful to deepen our understanding on the holographic duality between classical and quantum theories.

We are now proceeding to the application of stochastic quantization for fully non-equilibrium phenomena. As a preparation for this, we have presented an explicit check of the closed-time path (CTP) formalism for the non-interacting case. The time evolution of the expectation value of an operator is correctly reproduced from the initial time t_i to the final time t_f and it is reflected at $t = t_f$ that separates the forward path and the backward path. This indicates that the Feynman kernel is correctly calculable, and in principle, the time-dependence starting with arbitrary initial condition would be available from the convolution with the initial wave function. We are making progress in this direction including interaction effects.

Acknowledgments

K. F. would like to thank Jürgen Berges, Jan Pawłowski, and Dénes Sexty for useful conversations. K. F., Y. H., and T. O. were partially supported by JSPS KAKENHI Grant Number 24740169, 24740184, and 23740260, respectively. Y. H. was also supported by the RIKEN iTHES Project.

A One-loop self-energy calculation

We explicitly check if Eq. (22) holds for the one-loop self-energy. For notational convenience we define the inverse free propagator as

$$i \Delta^{-1} \equiv \omega^2 - \xi_{\mathbf{k}}^2 + i\epsilon. \quad (\text{A.1})$$

Then, using this notation, we can express the two-point function order by order in terms of the coupling λ . In the leading order (i.e., zeroth order in λ referred by a superscript (0) here), the left-hand side of Eq. (22) gives the free propagator by definition. The right-hand side takes a more non-trivial form that is

$$\overline{\langle \phi_{\mathbf{k}}(\theta) \phi_{\mathbf{k}'}(\theta) \rangle_{\eta}^{(0)}} = (2\pi)^d \delta(\mathbf{k} + \mathbf{k}') \Delta(\mathbf{k}) \frac{1}{\theta} \int_0^{\theta} d\theta' [1 - e^{-2\theta' \Delta^{-1}(\mathbf{k})}]. \quad (\text{A.2})$$

We can easily perform the θ -integration in the above expression to find that the free propagator (that is what our calculation is supposed to get) is multiplied by an extra factor, $1 + (\Delta/\theta)(e^{-2\theta \Delta^{-1}} - 1)/2$. The modulus of the deviation from the unity is now given by

$$\left| \frac{\Delta(\mathbf{k})}{\theta} \cdot \frac{e^{-2\theta \Delta^{-1}(\mathbf{k})} - 1}{2} \right| \leq \left| \frac{\Delta(\mathbf{k})}{\theta} \right| \cdot \left| \frac{e^{-2\theta \Delta^{-1}(\mathbf{k})} - 1}{2} \right| \leq \left| \frac{\Delta(\mathbf{k})}{\theta} \right| \leq \frac{1}{|\theta \epsilon|}. \quad (\text{A.3})$$

Sending θ to infinity while keeping a small but finite ϵ , we can safely drop this extra term and we can recover the free propagator as we should.

Now let us go to the next order that contributes to the one-loop diagram of the self-energy. Up to the first order in λ (referred by (1) here), we can perform tedious but straightforward calculations to reach eventually the following

expression,

$$\begin{aligned} \langle \phi_k(\theta) \phi_{k'}(\theta) \rangle_\eta^{(1)} &= -3i\lambda (2\pi)^d \delta^{(d)}(k+k') \Delta^2(k) \int \frac{d^d k_1}{(2\pi)^d} \Delta(k_1) \left[1 - e^{-2\theta\Delta^{-1}(k)} \right. \\ &\quad - 2e^{-2\theta\Delta^{-1}(k)} \theta \Delta^{-1}(k) - \frac{1}{1 - \Delta(k)\Delta^{-1}(k_1)} \left(e^{-2\theta\Delta^{-1}(k_1)} - e^{-2\theta\Delta^{-1}(k)} \right) \\ &\quad \left. - \Delta^{-1}(k) \Delta(k_1) e^{-2\theta\Delta^{-1}(k)} \left(e^{-2\theta\Delta^{-1}(k_1)} - 1 \right) \right]. \end{aligned} \quad (\text{A.4})$$

This complicated expression reduces to the standard expression of the self-energy once we take the $\theta \rightarrow \infty$ limit. Then, we can drop $e^{-2\theta\Delta^{-1}(k)}$ from the above and we correctly reproduce,

$$\lim_{\theta \rightarrow \infty} \langle \phi_k(\theta) \phi_{k'}(\theta) \rangle_\eta^{(1)} = (2\pi)^d \delta^{(d)}(k+k') \Delta^2(k) (-3i\lambda) \int \frac{d^d k_1}{(2\pi)^d} \Delta(k_1). \quad (\text{A.5})$$

In the same way as the previous example for the free propagator we can proceed to the θ -averaged calculation. The final results read,

$$\begin{aligned} \overline{\langle \phi_k(\theta) \phi_{k'}(\theta) \rangle_\eta^{(1)}} &= (2\pi)^d \delta^{(d)}(k+k') \Delta^2(k) (-3i\lambda) \int \frac{d^d k_1}{(2\pi)^d} \Delta(k_1) \\ &\quad \times \left[1 + e^{-2\theta\Delta^{-1}(k)} - \frac{\Delta(k)}{\theta} \left(1 - e^{-2\theta\Delta^{-1}(k)} \right) - \frac{1}{1 - \Delta(k)\Delta^{-1}(k_1)} \right. \\ &\quad \times \left(\frac{\Delta(k_1)}{\theta} \cdot \frac{1 - e^{-2\theta\Delta^{-1}(k_1)}}{2} - \frac{\Delta(k)}{\theta} \cdot \frac{1 - e^{-2\theta\Delta^{-1}(k)}}{2} \right) \\ &\quad - \Delta^{-1}(k) \Delta(k_1) \left(\frac{1}{\theta(\Delta^{-1}(k) + \Delta^{-1}(k_1))} \cdot \frac{1 - e^{-2\theta(\Delta^{-1}(k) + \Delta^{-1}(k_1))}}{2} \right. \\ &\quad \left. \left. - \frac{\Delta(k)}{\theta} \cdot \frac{1 - e^{-2\theta\Delta^{-1}(k)}}{2} \right) \right]. \end{aligned} \quad (\text{A.6})$$

Using the same inequality we can soon confirm that all additional terms in the square brackets are vanishing in the limit of $\theta \rightarrow \infty$ and then the above complicated expression simplifies to the standard one in Eq. (A.5).

B Diagonalization of the Hamiltonian in 0+1 dimensions

The one-dimensional Hamiltonian reduces to an as simple form as

$$H = \frac{\pi^2}{2} + \frac{\phi^2}{2} + \frac{\lambda}{4} \phi^4, \quad (\text{B.1})$$

where $m = 1$ and the commutation relation is $[\phi, \pi] = i$. This is a problem of quantum mechanics, which is numerically solvable by diagonalizing the

Hamiltonian. Here, we introduce the annihilation/creation operators as

$$a = \frac{1}{\sqrt{2}}(\phi + i\pi), \quad a^\dagger = \frac{1}{\sqrt{2}}(\phi - i\pi), \quad (\text{B.2})$$

which satisfy $[a, a^\dagger] = 1$. The harmonic part is $\pi^2/2 + \phi^2/2 = N + 1/2$ with the number operator $N = a^\dagger a$. Using $[N, a] = -a$ it is easy to show $[N, a^\dagger] = a^\dagger$, $a^2 a^\dagger^2 = (N+2)(N+1)$, and $a^\dagger^2 a^2 = N(N-1)$. Then we can expand the ϕ^4 term as

$$\begin{aligned} \phi^4 &= \frac{1}{4}(a + a^\dagger)^4 \\ &= \frac{1}{4}[a^4 + a^{\dagger 4} + 6N^2 + 6N + 3 + 2a^2(2N-1) + 2a^{\dagger 2}(2N+3)]. \end{aligned} \quad (\text{B.3})$$

We utilize the eigenvalue bases of N ; i.e., $|n\rangle$, which we can express as $|n\rangle \equiv (a^\dagger)^n |0\rangle / \sqrt{n!}$ using the creation operators. The matrix element of ϕ^4 is

$$\begin{aligned} \langle n | \phi^4 | m \rangle &= \frac{1}{4} \delta_{n,m} (6m^2 + 6m + 3) + \frac{1}{2} \delta_{n+2,m} \sqrt{(n+2)(n+1)(2n+3)} \\ &\quad + \frac{1}{2} \delta_{n,m+2} \sqrt{(m+2)(m+1)(2m+3)} \\ &\quad + \frac{1}{4} \delta_{n,m+4} \sqrt{(m+4)(m+3)(m+2)(m+1)} \\ &\quad + \frac{1}{4} \delta_{n+4,m} \sqrt{(n+4)(n+3)(n+2)(n+1)}. \end{aligned} \quad (\text{B.4})$$

Therefore, the matrix element of the Hamiltonian (B.1) is

$$\begin{aligned} \langle n | H | m \rangle &= \delta_{n,m} \left[m + \frac{1}{2} + \frac{\lambda}{16} (6m^2 + 6m + 3) \right] \\ &\quad + \frac{\lambda}{8} \delta_{n+2,m} \sqrt{(n+2)(n+1)(2n+3)} \\ &\quad + \frac{\lambda}{8} \delta_{n,m+2} \sqrt{(m+2)(m+1)(2m+3)} \\ &\quad + \frac{\lambda}{16} \delta_{n,m+4} \sqrt{(m+4)(m+3)(m+2)(m+1)} \\ &\quad + \frac{\lambda}{16} \delta_{n+4,m} \sqrt{(n+4)(n+3)(n+2)(n+1)}. \end{aligned} \quad (\text{B.5})$$

We can obtain the propagator in momentum space as

$$\begin{aligned} G(\omega) &= \int dt e^{i\omega t} \langle T \phi(t) \phi(0) \rangle \\ &= \int dt e^{i\omega t} \theta(t) \langle \phi(t) \phi(0) \rangle + \theta(-t) \langle \phi(0) \phi(t) \rangle \\ &= \sum_n \frac{2i\delta E_n}{\omega^2 - (\delta E_n)^2} \left| \langle E_n | \phi(0) | E_0 \rangle \right|^2, \end{aligned} \quad (\text{B.6})$$

where $|E_n\rangle$ is the eigenstate of H with the energy eigenvalue E_n . We also introduced a notation, $\delta E_n \equiv E_n - E_0$. The matrix element $\langle E_n|\phi(0)|E_0\rangle$ is expressed as

$$\begin{aligned}
\langle E_n|\phi(0)|E_0\rangle &= \sum_{m,l} \langle E_n|m\rangle \langle m|\phi|l\rangle \langle l|E_0\rangle \\
&= \sum_{m,l} \frac{1}{\sqrt{2}} \langle E_n|m\rangle \langle m|a + a^\dagger|l\rangle \langle l|E_0\rangle \\
&= \sum_{m,l} \frac{1}{\sqrt{2}} \langle E_n|m\rangle \langle l|E_0\rangle (\delta_{m+1,l}\sqrt{m+1} + \delta_{m,l+1}\sqrt{l+1}) \\
&= \sum_m \sqrt{\frac{m+1}{2}} (\langle E_n|m\rangle \langle m+1|E_0\rangle + \langle E_n|m+1\rangle \langle m|E_0\rangle) . \quad (\text{B.7})
\end{aligned}$$

We use the above form for the numerical calculation, which quickly converges to the exact answer. We can confirm that the above reduces to the free expression in the case of $\lambda = 0$ and thus $|E_n\rangle = |n\rangle$. Plugging $\langle E_n|\phi(0)|E_0\rangle = \delta_{n,1}/\sqrt{2}$ and $\delta E_n = n$ into the above, we can arrive at the following expression as

$$G(\omega) = \frac{i}{\omega^2 - 1} . \quad (\text{B.8})$$

Here we note that we use a unit with the mass $m = 1$ and if we retrieve the mass explicitly, the denominator is given by $\omega^2 - m^2$ in the above.

References

- [1] N. Brambilla, S. Eidelman, P. Foka, S. Gardner, A. Kronfeld, *et al.*, “QCD and strongly coupled gauge theories: challenges and perspectives,” [arXiv:1404.3723 \[hep-ph\]](#).
- [2] R. Gupta, “Introduction to lattice QCD: Course,” [arXiv:hep-lat/9807028 \[hep-lat\]](#).
- [3] H. Rothe, *Lattice Gauge Theories: An Introduction*. World Scientific Lecture Notes in Physics. World Scientific Publishing Company, Incorporated, 2012.
- [4] M. D’Elia and F. Negro, “ θ dependence of the deconfinement temperature in Yang-Mills theories,” *Phys. Rev. Lett.* **109** (2012) 072001, [arXiv:1205.0538 \[hep-lat\]](#).
- [5] A. Bazavov, T. Bhattacharya, M. Cheng, C. DeTar, H. Ding, *et al.*, “The chiral and deconfinement aspects of the QCD transition,” *Phys. Rev.* **D85** (2012) 054503, [arXiv:1111.1710 \[hep-lat\]](#).
- [6] S. Borsanyi, Z. Fodor, C. Hoelbling, S. D. Katz, S. Krieg, *et al.*, “Full result for the QCD equation of state with 2+1 flavors,” *Phys. Lett.* **B730** (2014) 99–104, [arXiv:1309.5258 \[hep-lat\]](#).

- [7] Z. Fodor and C. Hoelbling, “Light hadron masses from lattice QCD,” *Rev. Mod. Phys.* **84** (2012) 449, [arXiv:1203.4789 \[hep-lat\]](#).
- [8] Y. Nakahara, M. Asakawa, and T. Hatsuda, “Hadronic spectral functions in lattice QCD,” *Phys. Rev.* **D60** (1999) 091503, [arXiv:hep-lat/9905034 \[hep-lat\]](#).
- [9] M. Asakawa, T. Hatsuda, and Y. Nakahara, “Maximum entropy analysis of the spectral functions in lattice QCD,” *Prog. Part. Nucl. Phys.* **46** (2001) 459–508, [arXiv:hep-lat/0011040 \[hep-lat\]](#).
- [10] F. Karsch, E. Laermann, P. Petreczky, S. Stickan, and I. Wetzorke, “A Lattice calculation of thermal dilepton rates,” *Phys. Lett.* **B530** (2002) 147–152, [arXiv:hep-lat/0110208 \[hep-lat\]](#).
- [11] H.-T. Ding, A. Francis, O. Kaczmarek, F. Karsch, E. Laermann, *et al.*, “Thermal dilepton rate and electrical conductivity: An analysis of vector current correlation functions in quenched lattice QCD,” *Phys. Rev.* **D83** (2011) 034504, [arXiv:1012.4963 \[hep-lat\]](#).
- [12] A. Nakamura and S. Sakai, “Transport coefficients of gluon plasma,” *Phys. Rev. Lett.* **94** (2005) 072305, [arXiv:hep-lat/0406009 \[hep-lat\]](#).
- [13] H. B. Meyer, “A Calculation of the shear viscosity in SU(3) gluodynamics,” *Phys. Rev.* **D76** (2007) 101701, [arXiv:0704.1801 \[hep-lat\]](#).
- [14] H. B. Meyer, “A Calculation of the bulk viscosity in SU(3) gluodynamics,” *Phys. Rev. Lett.* **100** (2008) 162001, [arXiv:0710.3717 \[hep-lat\]](#).
- [15] G. Aarts, C. Allton, J. Foley, S. Hands, and S. Kim, “Spectral functions at small energies and the electrical conductivity in hot, quenched lattice QCD,” *Phys. Rev. Lett.* **99** (2007) 022002, [arXiv:hep-lat/0703008 \[HEP-LAT\]](#).
- [16] A. Amato, G. Aarts, C. Allton, P. Giudice, S. Hands, *et al.*, “Electrical conductivity of the quark-gluon plasma across the deconfinement transition,” *Phys. Rev. Lett.* **111** (2013) 172001, [arXiv:1307.6763 \[hep-lat\]](#).
- [17] M. Imada, A. Fujimori, and Y. Tokura, “Metal-insulator transitions,” *Rev. Mod. Phys.* **70** (1998) 1039–1263.
- [18] P. A. Lee, N. Nagaosa, and X.-G. Wen, “Doping a mott insulator: Physics of high-temperature superconductivity,” *Rev. Mod. Phys.* **78** (2006) 17–85.
- [19] S. R. White, “Density matrix formulation for quantum renormalization groups,” *Phys. Rev. Lett.* **69** (1992) 2863–2866.
- [20] U. Schollwöck, “The density-matrix renormalization group,” *Rev. Mod. Phys.* **77** (2005) 259–315.
- [21] A. Georges, G. Kotliar, W. Krauth, and M. J. Rozenberg, “Dynamical mean-field theory of strongly correlated fermion systems and the limit of infinite dimensions,” *Rev. Mod. Phys.* **68** (1996) 13–125.

- [22] H. Aoki, N. Tsuji, M. Eckstein, M. Kollar, T. Oka, and P. Werner, “Nonequilibrium dynamical mean-field theory and its applications,” [arXiv:1310.5329](#) [cond-mat].
- [23] J. Berges, S. Borsanyi, and C. Wetterich, “Prethermalization,” *Phys.Rev.Lett.* **93** (2004) 142002, [arXiv:hep-ph/0403234](#) [hep-ph].
- [24] M. Moeckel and S. Kehrein, “Crossover from adiabatic to sudden interaction quenches in the hubbard model: prethermalization and non-equilibrium dynamics,” *New J. Phys.* **12** (2010) 055016.
- [25] M. Eckstein, M. Kollar, and P. Werner, “Interaction quench in the hubbard model: Relaxation of the spectral function and the optical conductivity,” *Phys. Rev. B* **81** (2010) 115131.
- [26] M. A. Cazalilla and J. B. Marston, “Time-dependent density-matrix renormalization group: A systematic method for the study of quantum many-body out-of-equilibrium systems,” *Phys. Rev. Lett.* **88** (2002) 256403.
- [27] G. Vidal, A. J. Daley, C. Kollath, and U. Schollwoeck, “Time-dependent density-matrix renormalization-group using adaptive effective Hilbert spaces,” *J. Stat. Mech. Theor. Exp.* (2004) P04005.
- [28] S. White and A. Feiguin, “Real-time evolution using the density matrix renormalization group,” *Phys. Rev. Lett.* **93** (2004) no. 7, 1–4.
- [29] H.-P. Breuer and F. Petruccione, *The theory of open quantum systems*. Oxford University Press, Oxford, 2002.
- [30] J. Rammer, *Quantum Transport Theory*. Perseus Books, Massachusetts, 1998.
- [31] L. Kadanoff and G. Baym, *Quantum statistical mechanics: Green’s function methods in equilibrium and nonequilibrium problems*. Frontiers in physics. W.A. Benjamin, 1962.
- [32] L. Keldysh, “Diagram technique for nonequilibrium processes,” *Zh. Eksp. Teor. Fiz.* **47** (1964) 1515–1527.
- [33] J. S. Schwinger, “Brownian motion of a quantum oscillator,” *J. Math. Phys.* **2** (1961) 407–432.
- [34] P. Werner, T. Oka, and A. J. Millis, “Diagrammatic monte carlo simulation of nonequilibrium systems,” *Phys. Rev. B* **79** (2009) 035320.
- [35] L. Mühlbacher and E. Rabani, “Real-time path integral approach to nonequilibrium many-body quantum systems,” *Phys. Rev. Lett.* **100** (2008) 176403.
- [36] J. K. Freericks, V. M. Turkowski, and V. Zlatić, “Nonequilibrium dynamical mean-field theory,” *Phys. Rev. Lett.* **97** (2006) 266408.
- [37] M. Cross and P. Hohenberg, “Pattern formation outside of equilibrium,” *Rev. Mod. Phys.* **65** (1993) 851.

- [38] K. Avila, D. Moxey, A. de Lozar, M. Avila, D. Barkley, and B. Hof, “The onset of turbulence in pipe flow,” *Science* **333** (2011) no. 6039, 192–196.
- [39] O. Aharony, S. S. Gubser, J. M. Maldacena, H. Ooguri, and Y. Oz, “Large N field theories, string theory and gravity,” *Phys. Rept.* **323** (2000) 183–386, [arXiv:hep-th/9905111](#) [[hep-th](#)].
- [40] D. Polarski and A. A. Starobinsky, “Semiclassicality and decoherence of cosmological perturbations,” *Class. Quant. Grav.* **13** (1996) 377–392, [arXiv:gr-qc/9504030](#) [[gr-qc](#)].
- [41] D. Son, “Classical preheating and decoherence,” [arXiv:hep-ph/9601377](#) [[hep-ph](#)].
- [42] S. Y. Khlebnikov and I. Tkachev, “Classical decay of inflaton,” *Phys. Rev. Lett.* **77** (1996) 219–222, [arXiv:hep-ph/9603378](#) [[hep-ph](#)].
- [43] J. M. Cornwall, R. Jackiw, and E. Tomboulis, “Effective action for composite operators,” *Phys. Rev.* **D10** (1974) 2428–2445.
- [44] E. Nelson, “Derivation of the Schrodinger equation from Newtonian mechanics,” *Phys. Rev.* **150** (1966) 1079–1085.
- [45] G. Parisi and Y.-s. Wu, “Perturbation theory without gauge fixing,” *Sci. Sin.* **24** (1981) 483.
- [46] P. H. Damgaard and H. Huffel, “Stochastic quantization,” *Phys. Rept.* **152** (1987) 227.
- [47] M. Namiki, “Basic ideas of stochastic quantization,” *Prog. Theor. Phys. Suppl.* **111** (1993) 1–41.
- [48] P. M. Chesler and L. G. Yaffe, “Horizon formation and far-from-equilibrium isotropization in supersymmetric Yang-Mills plasma,” *Phys. Rev. Lett.* **102** (2009) 211601, [arXiv:0812.2053](#) [[hep-th](#)].
- [49] P. M. Chesler and L. G. Yaffe, “Boost invariant flow, black hole formation, and far-from-equilibrium dynamics in $N = 4$ supersymmetric Yang-Mills theory,” *Phys. Rev.* **D82** (2010) 026006, [arXiv:0906.4426](#) [[hep-th](#)].
- [50] D. Grumiller and P. Romatschke, “On the collision of two shock waves in AdS(5),” *JHEP* **0808** (2008) 027, [arXiv:0803.3226](#) [[hep-th](#)].
- [51] V. Balasubramanian, A. Bernamonti, J. de Boer, N. Copland, B. Craps, *et al.*, “Thermalization of strongly coupled field theories,” *Phys. Rev. Lett.* **106** (2011) 191601, [arXiv:1012.4753](#) [[hep-th](#)].
- [52] V. Balasubramanian, A. Bernamonti, J. de Boer, N. Copland, B. Craps, *et al.*, “Holographic thermalization,” *Phys. Rev.* **D84** (2011) 026010, [arXiv:1103.2683](#) [[hep-th](#)].
- [53] M. P. Heller, R. A. Janik, and P. Witaszczyk, “The characteristics of thermalization of boost-invariant plasma from holography,” *Phys. Rev. Lett.* **108** (2012) 201602, [arXiv:1103.3452](#) [[hep-th](#)].

- [54] K. Hashimoto, N. Iizuka, and T. Oka, “Rapid thermalization by baryon injection in gauge/gravity duality,” *Phys. Rev.* **D84** (2011) 066005, [arXiv:1012.4463 \[hep-th\]](#).
- [55] A. Polkovnikov, “Phase space representation of quantum dynamics,” *Annals of Phys.* **325** (2010) 1790–1852.
- [56] P. Romatschke and R. Venugopalan, “Collective non-Abelian instabilities in a melting color glass condensate,” *Phys. Rev. Lett.* **96** (2006) 062302, [arXiv:hep-ph/0510121 \[hep-ph\]](#).
- [57] P. Romatschke and R. Venugopalan, “The Unstable Glasma,” *Phys. Rev.* **D74** (2006) 045011, [arXiv:hep-ph/0605045 \[hep-ph\]](#).
- [58] K. Fukushima, F. Gelis, and L. McLerran, “Initial singularity of the little bang,” *Nucl. Phys.* **A786** (2007) 107–130, [arXiv:hep-ph/0610416 \[hep-ph\]](#).
- [59] F. Gelis, T. Lappi, and R. Venugopalan, “High energy scattering in Quantum Chromodynamics,” *Int. J. Mod. Phys.* **E16** (2007) 2595–2637, [arXiv:0708.0047 \[hep-ph\]](#).
- [60] K. Dusling, T. Epelbaum, F. Gelis, and R. Venugopalan, “Role of quantum fluctuations in a system with strong fields: Onset of hydrodynamical flow,” *Nucl. Phys.* **A850** (2011) 69–109, [arXiv:1009.4363 \[hep-ph\]](#).
- [61] T. Epelbaum and F. Gelis, “Role of quantum fluctuations in a system with strong fields: Spectral properties and Thermalization,” *Nucl. Phys.* **A872** (2011) 210–244, [arXiv:1107.0668 \[hep-ph\]](#).
- [62] K. Dusling, T. Epelbaum, F. Gelis, and R. Venugopalan, “Instability induced pressure isotropization in a longitudinally expanding system,” *Phys. Rev.* **D86** (2012) 085040, [arXiv:1206.3336 \[hep-ph\]](#).
- [63] K. Fukushima and F. Gelis, “The evolving Glasma,” *Nucl. Phys.* **A874** (2012) 108–129, [arXiv:1106.1396 \[hep-ph\]](#).
- [64] K. Fukushima, “Turbulent pattern formation and diffusion in the early-time dynamics in the relativistic heavy-ion collision,” *Phys. Rev.* **C89** (2014) 024907, [arXiv:1307.1046 \[hep-ph\]](#).
- [65] J. Berges, K. Boguslavski, S. Schlichting, and R. Venugopalan, “Turbulent thermalization process in heavy-ion collisions at ultrarelativistic energies,” [arXiv:1303.5650 \[hep-ph\]](#).
- [66] J. Berges, K. Boguslavski, S. Schlichting, and R. Venugopalan, “Universal attractor in a highly occupied non-Abelian plasma,” [arXiv:1311.3005 \[hep-ph\]](#).
- [67] J. Berges, K. Boguslavski, S. Schlichting, and R. Venugopalan, “Basin of attraction for turbulent thermalization and the range of validity of classical-statistical simulations,” [arXiv:1312.5216 \[hep-ph\]](#).

- [68] V. Kasper, F. Hebenstreit, and J. Berges, “Fermion production from real-time lattice gauge theory in the classical-statistical regime,” [arXiv:1403.4849](#) [[hep-ph](#)].
- [69] T. Epelbaum, F. Gelis, and B. Wu, “Non-renormalizability of the classical statistical approximation,” [arXiv:1402.0115](#) [[hep-ph](#)].
- [70] K. Fukushima and T. Hayata, “Schwinger mechanism with stochastic quantization,” [arXiv:1403.4177](#) [[hep-th](#)].
- [71] F. Gelis and N. Tanji, “Formulation of the Schwinger mechanism in classical statistical field theory,” *Phys. Rev.* **D87** (2013) no. 12, 125035, [arXiv:1303.4633](#) [[hep-ph](#)].
- [72] J. Berges and I.-O. Stamatescu, “Simulating nonequilibrium quantum fields with stochastic quantization techniques,” *Phys. Rev. Lett.* **95** (2005) 202003, [arXiv:hep-lat/0508030](#) [[hep-lat](#)].
- [73] J. Berges, S. Borsanyi, D. Sexty, and I.-O. Stamatescu, “Lattice simulations of real-time quantum fields,” *Phys. Rev.* **D75** (2007) 045007, [arXiv:hep-lat/0609058](#) [[hep-lat](#)].
- [74] J. Berges and D. Sexty, “Real-time gauge theory simulations from stochastic quantization with optimized updating,” *Nucl. Phys.* **B799** (2008) 306–329, [arXiv:0708.0779](#) [[hep-lat](#)].
- [75] G. Parisi, “On complex probabilities,” *Phys. Lett.* **B131** (1983) 393–395.
- [76] H. Huffel and H. Rumpf, “Stochastic quantization in Minkowski space,” *Phys. Lett.* **B148** (1984) 104–110.
- [77] S. Muroya, A. Nakamura, C. Nonaka, and T. Takaishi, “Lattice QCD at finite density: An Introductory review,” *Prog. Theor. Phys.* **110** (2003) 615–668, [arXiv:hep-lat/0306031](#) [[hep-lat](#)].
- [78] G. Aarts, “Complex Langevin dynamics and other approaches at finite chemical potential,” *PoS LATTICE2012* (2012) 017, [arXiv:1302.3028](#) [[hep-lat](#)].
- [79] G. Aarts, L. Bongiovanni, E. Seiler, D. Sexty, and I.-O. Stamatescu, “Controlling complex Langevin dynamics at finite density,” *Eur. Phys. J.* **A49** (2013) 89, [arXiv:1303.6425](#) [[hep-lat](#)].
- [80] **AuroraScience Collaboration** Collaboration, M. Cristoforetti, F. Di Renzo, and L. Scorzato, “New approach to the sign problem in quantum field theories: High density QCD on a Lefschetz thimble,” *Phys. Rev.* **D86** (2012) 074506, [arXiv:1205.3996](#) [[hep-lat](#)].
- [81] H. Fujii, D. Honda, M. Kato, Y. Kikukawa, S. Komatsu, *et al.*, “Hybrid Monte Carlo on Lefschetz thimbles - A study of the residual sign problem,” *JHEP* **1310** (2013) 147, [arXiv:1309.4371](#) [[hep-lat](#)].

- [82] M. Cristoforetti, F. Di Renzo, A. Mukherjee, and L. Scorzato, “Quantum field theories on the Lefschetz thimble,” [arXiv:1312.1052 \[hep-lat\]](#).
- [83] A. Mukherjee and M. Cristoforetti, “Lefschetz thimble Monte Carlo for many body theories: application to the repulsive Hubbard model away from half filling,” [arXiv:1403.5680 \[cond-mat.str-el\]](#).
- [84] M. Cristoforetti, F. Di Renzo, G. Eruzzi, A. Mukherjee, C. Schmidt, *et al.*, “An efficient method to compute the residual phase on a Lefschetz thimble,” [arXiv:1403.5637 \[hep-lat\]](#).
- [85] N. Landsman and C. van Weert, “Real and imaginary time field theory at finite temperature and density,” *Phys. Rept.* **145** (1987) 141.
- [86] W. Grimus and H. Huffel, “Perturbation theory from stochastic quantization of scalar fields,” *Z. Phys.* **C18** (1983) 129.
- [87] H. Huffel and P. Landshoff, “Stochastic diagrams and Feynman diagrams,” *Nucl. Phys.* **B260** (1985) 545.
- [88] G. Aarts, P. Giudice, and E. Seiler, “Localised distributions and criteria for correctness in complex Langevin dynamics,” *Annals Phys.* **337** (2013) 238–260, [arXiv:1306.3075 \[hep-lat\]](#).
- [89] G. Aarts, F. A. James, J. M. Pawłowski, E. Seiler, D. Sexty, *et al.*, “Stability of complex Langevin dynamics in effective models,” *JHEP* **1303** (2013) 073, [arXiv:1212.5231 \[hep-lat\]](#).
- [90] G. Aarts, E. Seiler, and I.-O. Stamatescu, “The Complex Langevin method: When can it be trusted?,” *Phys. Rev.* **D81** (2010) 054508, [arXiv:0912.3360 \[hep-lat\]](#).
- [91] G. Aarts, F. A. James, E. Seiler, and I.-O. Stamatescu, “Complex Langevin: etiology and diagnostics of its main problem,” *Eur. Phys. J.* **C71** (2011) 1756, [arXiv:1101.3270 \[hep-lat\]](#).
- [92] R. Feynman and A. Hibbs, *Quantum mechanics and path integrals*. International series in pure and applied physics. McGraw-Hill, 1965.
- [93] W. H. Press, S. A. Teukolsky, W. T. Vetterling, and B. P. Flannery, *Numerical Recipes 3rd Edition: The Art of Scientific Computing*. Cambridge University Press, New York, NY, USA, 3 ed., 2007.
- [94] G. Aarts, F. A. James, E. Seiler, and I.-O. Stamatescu, “Adaptive stepsize and instabilities in complex Langevin dynamics,” *Phys. Lett.* **B687** (2010) 154–159, [arXiv:0912.0617 \[hep-lat\]](#).